Incorporation of Iterative Forward Modeling Into the Principle Phase Decomposition Algorithm for Accurate Source Wave and Reflection Series Estimation

Erick Baziw, *Senior Member, IEEE*

***Abstract*—This paper outlines a more powerful formulation of a previously published new concept in blind seismic deconvolution, referred to as principle phase decomposition (PPD). In this new PPD filter formulation, an iterative forward modeling (IFM) algorithm is incorporated, which facilitates the estimation of parameters defining the source wave (i.e., dominant frequency, phase, and decay) and the overlapping source waves (i.e., reflection coefficients' corresponding arrival times and amplitudes). This IFM integrated PPD algorithm allows for a significantly more accurate approach in estimating the source wave and corresponding reflection series compared to the previously published technique of sequentially estimating the source wave and overlapping source waves utilizing a Rao–Blackwellized particle filter. In general terms, the source wave is modeled as an amplitude-modulated sinusoid, and the overlapping source waves are treated as known inputs within the Kalman filter formulation based on the current source wave and reflection series IFM parameter estimates. The source wave and reflection series parameters are obtained by iteratively minimizing a cost function defined to be the rms difference between the measured seismogram and the synthesized seismogram within the IFM algorithm.**

***Index Terms*—Blind deconvolution, iterative forward modeling (IFM), Kalman filter, parameter estimation.**

I. Introduction

IN SEISMOLOGY, the most important seismic model is, in general, written as [1]

$$z(t) = S(t) * \mu(t) + v(t) \tag{1}$$

where

- $z(t)$ measured seismogram;
- $S(t)$ seismic wave, which is a superposition of the Earth and instrument responses;
- $\mu(t)$ reflectivity of the Earth, which consists of all primary reflections as well as all surface and internal multiples;
- $v(t)$ additive noise, generally taken to be white with a Gaussian pdf;
- $*$ denotes the convolution operation.

Manuscript received November 6, 2009; revised January 15, 2010, April 8, 2010, and May 17, 2010.

The author is with Baziw Consulting Engineers Ltd., 3943 West 32nd Avenue, Vancouver, BC V6S 1Z4, Canada (e-mail: ebaziw@bcengineers.com).

Color versions of one or more of the figures in this paper are available online at http://ieeexplore.ieee.org.

Digital Object Identifier 10.1109/TGRS.2010.2058122

A fundamental task for the seismologist is to estimate the impedance at depth from the recorded seismogram. A commonly adopted simple model in applied seismology is that of a horizontally layered 1-D Earth, referred to as the Goupillaud layered medium [1]. Here, the impedance of the kth layer of the pancake Earth model is defined as

$$\varepsilon_k = \rho_k V_k \tag{2}$$

where ρ_k and V_k are the density and velocity in the kth layer, respectively. The relationship between ε_k and μ_k, which is the reflection coefficient (assuming only a primary reflection) of the kth layer, is

$$\mu_k = \frac{\varepsilon_{k+1} - \varepsilon_k}{\varepsilon_{k+1} + \varepsilon_k} \tag{3}$$

Rearranging (3) gives

$$\varepsilon_{k+1} = \varepsilon_k \left(\frac{1+\mu_k}{1-\mu_k} \right) = \varepsilon_1 \prod_{j=1}^{k} \left(\frac{1+\mu_j}{1-\mu_j} \right). \tag{4}$$

Therefore, it is required to estimate the reflection series μ_k in order to determine ε_k. In extracting the reflection series, therefore, the source wave must first be estimated and then deconvolved from the recorded seismogram.

An alternative mathematical representation of the recorded time series $z(t)$, defined in (1), is given as

$$z(t) = \int_o^t \mu(\tau) S(t-\tau) d\tau + v(t). \tag{5}$$

The discrete representation of (5) is given as

$$z(k) = \sum_{i=1}^{k} \mu(i) S\left(k-(i-1)\right) + v(k), \quad k = 1, 2, \ldots, N \tag{6}$$

where N is the length of the time series.

As previously stated, the primary goal of seismic deconvolution is to remove the characteristics of the source wave from the recorded seismic time series so that one is ideally left with only the reflection coefficients. The reflection coefficients identify and quantify the impedance mismatches between different geological layers that are of great interest to the geophysicist.

A very challenging and yet common seismic deconvolution problem is when the source wave is unknown and has the potential for time variation. This is referred to as blind seismic deconvolution (BSD), and it identifies the case where we have one known (measured seismogram with additive noise) and two unknowns (source wave and reflection coefficients).

There are many techniques in seismic deconvolution that can be implemented so that an optimal estimate is made of the Earth model. The majority of the standard seismic deconvolution methods utilize the steady-state Wiener digital filter that assumes a minimum phase source wave [2]. Other techniques implement inverse theory, minimum entropy deconvolution, adaptive deconvolution, complex cepstrum deconvolution, and independent component analysis. Many of these deconvolution techniques are ad hoc in nature [3], [4], they are affected by the band-limited nature of the source wave, they are highly susceptible to additive measurement noise, and they assume that the source wave is stationary.

In [5], an innovative and powerful algorithm for solving the BSD problem was introduced based on the Bayesian recursive estimation (BRE). The algorithm is referred to as principle phase decomposition (PPD). In this algorithm, all of the associated filters of BRE (hidden Markov model filter, Kalman Filter, particle filter, Rao–Blackwellized particle filter (RBPF), and jump Markov systems) have been incorporated. Moreover, the source waves are modeled as amplitude-modulated sinusoids (AMSs) embedded within Gauss–Markov measurement noise, and the blind deconvolution is carried out by initially determining the seismogram's principle phase components. Once the principle phases are determined, an RBPF algorithm is utilized to separate the corresponding overlapping source waves.

The PPD algorithm outlined in [5] was shown to have many advantages since it allows for simple filter formulation with minimal parameter specification, and it is conducive to BSD. Moreover, the assumption of the minimum phase source wave is not required. The algorithm avoids problems associated with band-limited source waves when carrying out frequency-domain deconvolution and easily handles nonstationary source waves while providing time-variant estimations of the source wave. Finally, reflection coefficients are not required to be represented by discrete state levels, and a whiteness assumption governing the reflection coefficient series is not required.

However, the major drawback of the PPD algorithm outlined in [5] is that the investigator is required to initially specify the phases of the overlapping source waves. To circumvent this shortcoming, a variant of the PPD technique, which is the so-called PPD-WE algorithm, was outlined [6]. In this algorithm, the overlapping source waves are sequentially and chronologically extracted from the seismogram under analysis. As clearly outlined in [6], a limitation of the PPD-WE technique is that it has difficulty if either the overlapping source waves have or the overall seismogram response has phase components similar to the source wave to be extracted. Furthermore, there is a gradual decrease in the quality of the estimated source waves due to the fact that any errors generated during the source wave extraction process are propagated as the seismogram is sequentially and chronologically processed.

To overcome the aforementioned PPD algorithm limitations, a new formulation is outlined in this paper, whereby an iterative forward modeling (IFM) algorithm is incorporated into the PPD technique, which allows for a significantly more accurate estimation of the source wave and corresponding reflection coefficients. This formulation of the PPD algorithm is referred to as the PPD-IFM technique. A fundamental component of the PPD-IFM algorithm (and all variations of the PPD algorithm) is that the overlapping source waves are modeled as AMSs and that the discrete convolution operation outlined in (6) can be represented as the summation of several source waves of differing arrival times. The formulation of the PPD algorithm [5], [6] has been credited with the introduction of particle filtering into BSD [7].

II. Background

A. AMS

In all variations of the PPD algorithm, an innovative model of the source wave is utilized. This source wave model is referred to as the AMS [5], [6], [8], [9]. The AMS is demonstrated to be a highly robust and accurate approximation of many analytical representations of seismic source waves such as the exponentially decaying cyclic waveform, the mixed-phase Berlage wave, the zero-phase Ricker wave, and the zero-phase Klauder wave. In addition, the AMS wave has proven to be very accurate in modeling seismic data acquired during passive seismic monitoring and vertical seismic profiling.

For completeness, a review of the AMS wave is given along with the simulated and real examples. The mathematical representation of the AMS source wave is given as

$$x_1(t) = x_2(t)\sin[\omega t + \varphi] \tag{7}$$

where $x_1(t)$ is an approximation of the seismic source wave, $x_2(t)$ is the seismic wave's amplitude-modulating term (AMT), ω is the dominant frequency of the wave, and φ is the corresponding phase.

In [5], the robustness of the AMS model was demonstrated by considering the zero-phase Ricker wave. The Ricker wave is mathematically represented in the time domain as

$$f(t) = A_0\left(1-2\pi^2 v_M^2 (t-t_0)^2\right) e^{-\left(\pi^2 v_M^2 (t-t_0)^2\right)}, \quad t \geq t_0 \tag{8}$$

where $A_0 \equiv$ wave maximum amplitude (centered between two flanking lobes), $v_M \equiv$ dominant or peak frequency of the Ricker wave, and $t_0 \equiv$ wave arrival time of the maximum amplitude. Although the Ricker wave has a peak frequency, it does not have a specific sinusoidal term, and as was shown in [5], the AMS model was able to reconstruct the desired wave by applying an appropriate AMT.

Another analytical model of the seismic source wave is the Berlage wave. The Berlage wave is defined as

$$w(t) = AH(t)t^n e^{-\alpha t}\cos(2\pi f t + \phi) \tag{9}$$

where $H(t)$ is the Heaviside unit step function [$H(t) = 0$ for $t \leq 0$ and $H(t) = 1$ for $t > 0$]. The amplitude-modulation component is controlled by two factors: the exponential decay

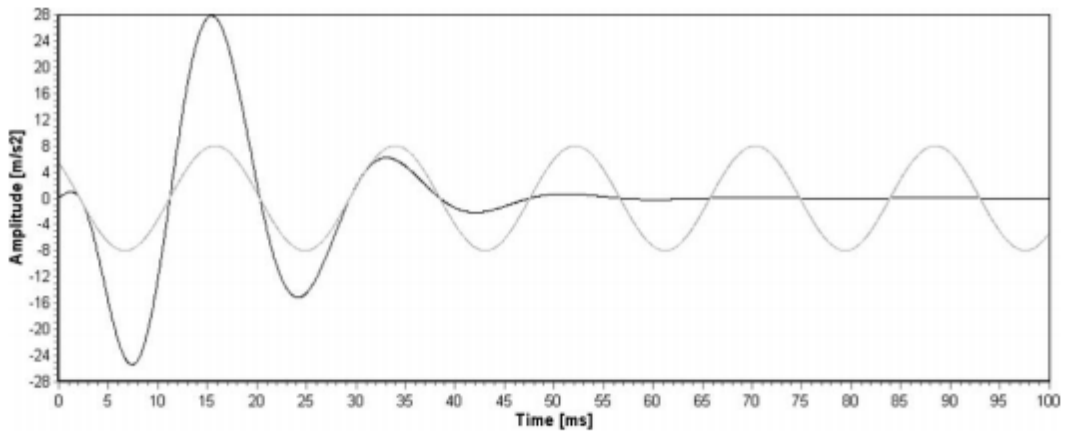

Fig. 1. Berlage wave with superimposed 55-Hz sinusoid.

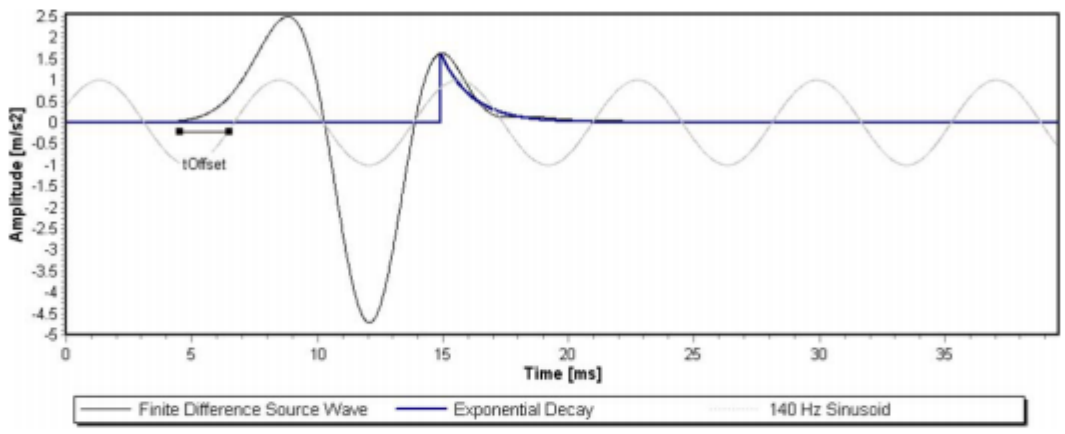

Fig. 2. Finite-difference source wave with a superimposed 140-Hz sinusoid and an exponential decay with a rate of 0.8/ms.

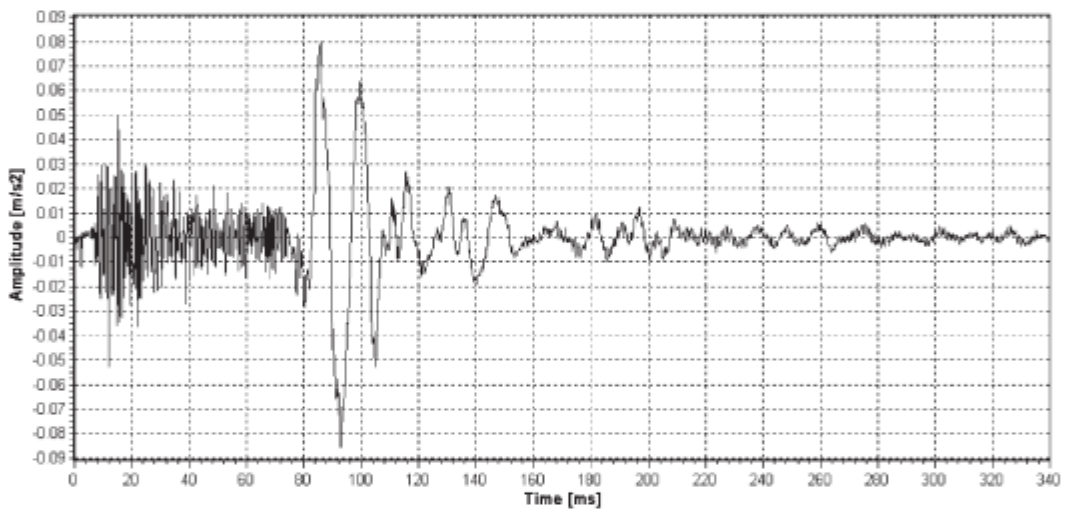

Fig. 3. AMS real data example recorded during an SCPT.

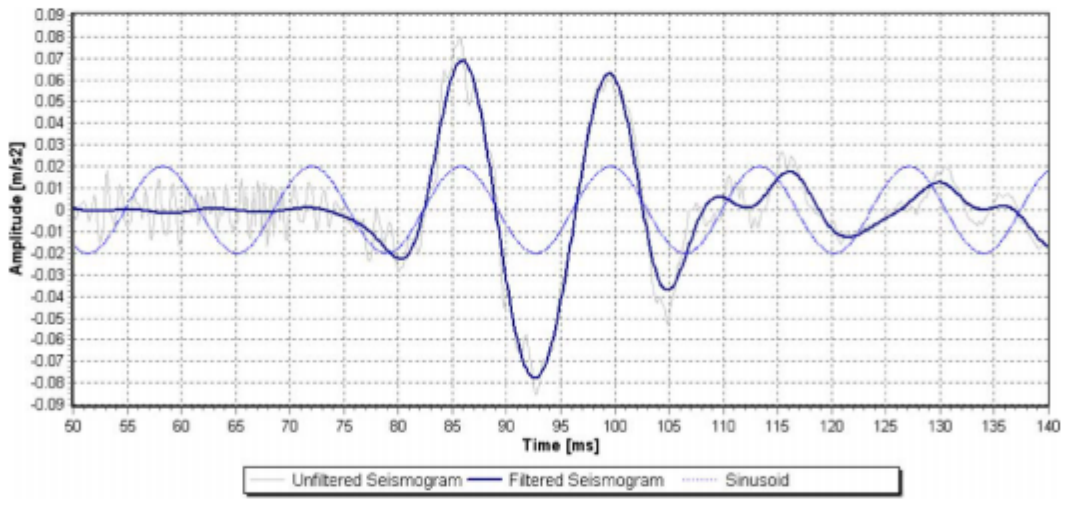

Fig. 4. Seismic trace in Fig. 3 with a 10–150-Hz frequency filter applied and a 73-Hz sinusoid superimposed.

term α and the time exponent n. These parameters are considered to be nonnegative real constants. Fig. 1 shows a Berlage wave with $f = 55$ Hz, $n = 2$, $\alpha = 168$, and $\phi = 168°$. Superimposed upon the Berlage wave is a scaled 55-Hz sinusoid with zero crossing at 11.2 ms. As shown in Fig. 1, the Berlage source wave is an AMS.

Amini and Howie [11], [12] utilized a finite-difference program (FLAC) to model downhole seismic source waves. Fig. 2 shows the simulated source wave generated by Amini and

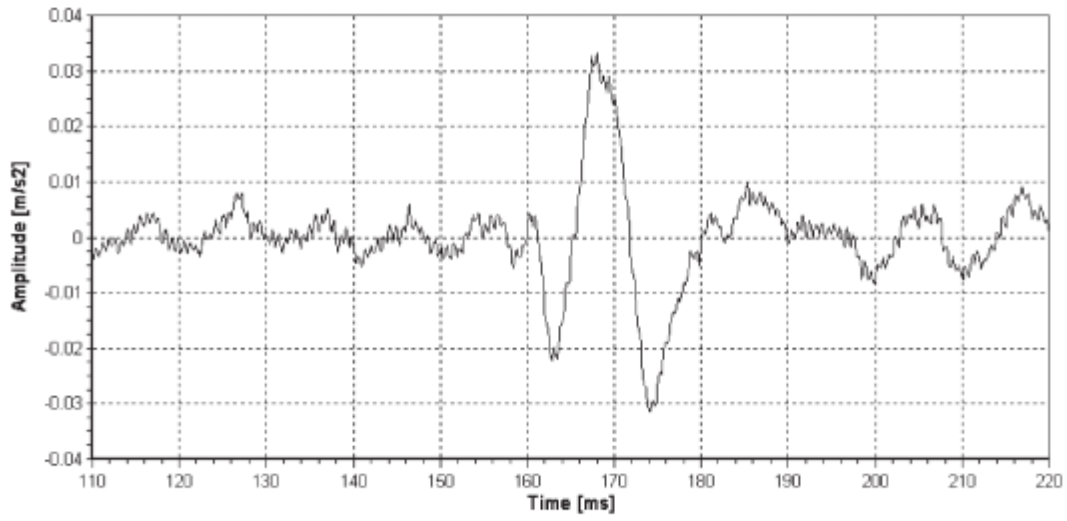

Fig. 5. AMS real data example recorded at a depth of 30 m during an SCPT.

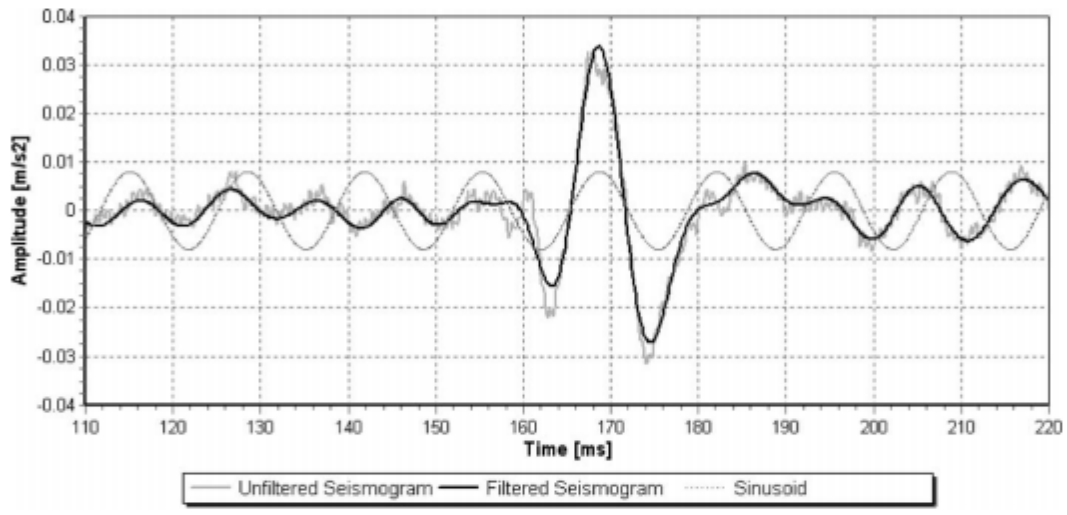

Fig. 6. Seismic trace in Fig. 5 with a 10–150-Hz frequency filter applied and a 74-Hz sinusoid superimposed.

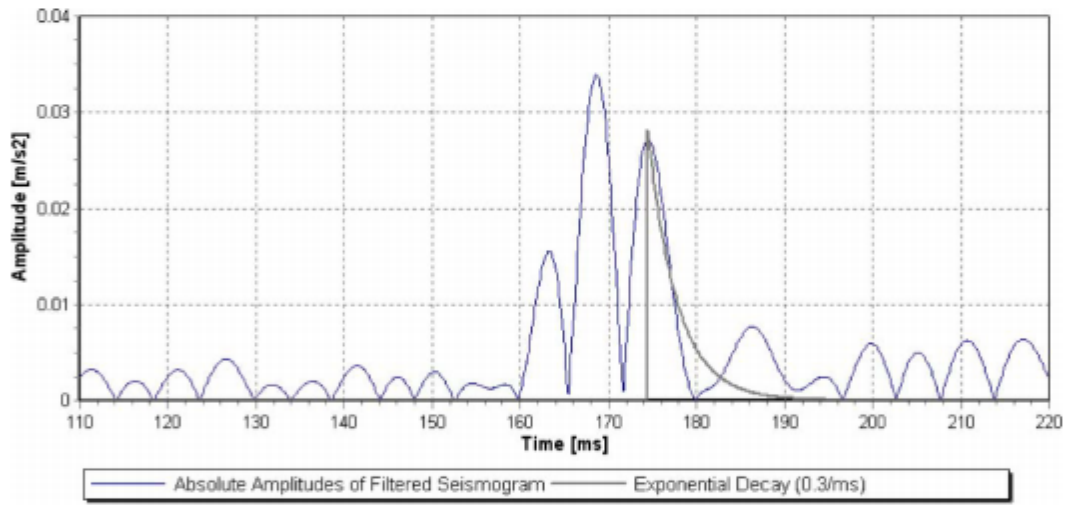

Fig. 7. Absolute amplitudes of the filtered trace shown in Fig. 6 with a superimposed exponential decay with a rate of 0.3/ms.

Howie obtained by personal communication. The source wave shown in Fig. 2 was generated by assuming a uniform halfspace with an *in situ* shear wave velocity of 180 m/s and a sampling interval of 0.02 ms. Superimposed upon the finite-difference source wave is a scaled 140-Hz sinusoid with zero crossing at 10.3 ms. Also, superimposed upon the source wave shown in Fig. 2 is an exponential decay peaking at 15 ms and decaying at an exponential rate of 0.8/ms. Fig. 2 shows the three parameters which define the AMS source wave. These parameters are outlined as follows:

- ω source wave's dominant frequency;
- t_{Offset} offset time from the arrival time of the source wave (t_0) when the sinusoidal component commences. This parameter is inherently related to the phase φ due to the fact that the arrival time of the source wave (t_0) is readily obtained from the seismogram;
- h exponential decay rate of the source wave.

AMS real data examples are provided from downhole seismic data captured during a seismic cone penetration test (SCPT) [13]–[15]. The SCPT is utilized extensively in geotechnical *in situ* P-wave and S-wave site characterization. The SCPT real data examples were captured with high-precision and high-bandwidth (1 Hz–10 kHz) piezoelectric accelerometers that have an operational amplifier integrated within the sensor [14]. The piezoelectric accelerometers have highly desirable rise and decay times of approximately 5 μs. These fast rise and decay times result in recorded traces where the input of acoustic waves and ambient noise are recorded with minimal or no sensor distortion [14].

Fig. 3 shows the noisy SCPT data recorded at a depth of 15 m. The high noise energy is due to the high-frequency rod noise traveling down the steel extension rods and due to the close radial proximity of the source [13]–[16]. Fig. 4 shows the seismic data shown in Fig. 3 superimposed upon the same seismic trace filtered with a zero-phase-shift eighth-order Butterworth 10–150-Hz bandpass filter applied [15]. Also, superimposed upon the filtered seismic trace is a 73-Hz sinusoid. As shown in Fig. 4, the real SCPT source wave can be modeled as an AMS.

Fig. 5 illustrates another real data example of a noisy SCPT seismic data trace recorded at a depth of 30 m. Fig. 6 illustrates the seismic data shown in Fig. 5 superimposed upon the same seismic trace filtered with a zero-phase-shift eighth-order Butterworth 10–150-Hz bandpass filter applied. Also, superimposed upon the filtered seismic trace is a 74-Hz sinusoid. Fig. 7 illustrates the absolute amplitudes of the filtered trace shown in Fig. 6 with an exponential decay peaking at 174.5 ms and decaying at an exponential rate of 0.3/ms. As shown in Figs. 6 and 7, the real SCPT source wave can be modeled as an AMS.

B. Kalman Filter Governing Equations

In [3]–[6], [8], [9], and [12], the details of the BRE technique of Kalman filtering (KF) are outlined along with the governing equations. The KF governing equations for a known input are outlined in [5, Table I] .

It is assumed that there are very low measurement noise and process noise (i.e., $\boldsymbol{Q}_k \to 0$ and $\boldsymbol{R}_k \to 0$) within the PPD-IFM algorithm. This is due to the fact that the seismic data can be preprocessed, as shown in Figs. 4 and 6, prior to inputting the seismogram into the PPD-IFM algorithm. For the case where $\boldsymbol{Q}_k \to 0$ and $\boldsymbol{R}_k \to 0$ and for a single-state estimation problem (only estimating the AMT component of the AMS source wave), the KF governing equations are simplified as outlined in Table I.

In Table I, x_k denotes the state (AMT) to be estimated, F_{k-1} denotes the state transition matrix which describes the system dynamics, u_{k-1} denotes a known deterministic time-varying input, Λ_{k-1} describes the relationship between x_k and u_{k-1}, and H_k defines the relationship between the state and the available measurement (seismogram time series). The implementation of (10) to (15) is outlined in detail in [3]–[6], [8], [9], and [12]. In general terms, (12) and (13) are used to predict the state and measurement, innovation (14) is then calculated (difference between the actual and predicted measurements), and the state is updated by adding the predicted value (12) with the weighted innovation Δ_k / H_k.

TABLE I
SIMPLIFIED KF GOVERNING EQUATIONS FOR KNOWN INPUTS

Description	Mathematical Representation	Eq.
System equation.	$x_k = F_{k-1} x_{k-1} + \Lambda_{k-1} u_{k-1}$	10
Measurement equation.	$z_k = H_k x_k$	11
State estimate extrapolation.	$\hat{x}_{k\|k-1} = F_{k-1} \hat{x}_{k-1\|k-1} + \Lambda_{k-1} u_{k-1}$	12
Measurement extrapolation.	$\hat{z}_k = H_k \hat{x}_{k\|k-1}$	13
Innovation.	$\Delta_k = z_k - \hat{z}_k$	14
State estimate update.	$\hat{x}_{k\|k} = \hat{x}_{k\|k-1} + \Delta_k / H_k$	15

C. IFM

IFM is a parameter estimation technique that is based on iteratively adjusting the parameters until a user-specified cost function is minimized. The desired parameter estimates are defined as those which minimize the user-specified cost function.

The IFM technique which is utilized within the PPD-IFM algorithm is the downhill simplex method (DSM) originally developed by Nelder and Mead [17]. The DSM in multidimensions has the important property of not requiring derivatives of function evaluations, and it can minimize nonlinear functions of more than one independent variables. Although it is not the most efficient optimization procedure, the DSM is versatile, robust, and simple to implement.

A simplex defines the most elementary geometric figure of a given dimension: a line in one dimension, a triangle in two dimensions, a tetrahedron in three, etc. Therefore, in an N-dimensional space, the simplex is a geometric figure that consists of $N + 1$ fully interconnected vertices [16]–[18]. For example, in determining the location of a seismic event, a 3-D space is searched, so the simplex is a tetrahedron with four vertices.

The DSM starts at $N + 1$ vertices that form the initial simplex. The initial simplex vertices are chosen so that the simplex occupies a good portion of the solution space. In addition, it is also required that a scalar cost function be specified at each vertex of the simplex.

The general idea of the minimization is to keep the minimum within the simplex during the optimization, decreasing the volume of the simplex at the same time. The DSM searches for the minimum of the cost function by taking a series of steps, each time moving a point in the simplex away from where the cost function is largest. The simplex moves in space by variously reflecting, expanding, contracting, or shrinking. The

simplex size is continuously changed and mostly diminished so that, finally, it is small enough to contain the minimum with the desired accuracy.

The DSM incorporates the following basic steps [16], [18].

1) Specify the initial simplex vertices.
2) Specify the cost function at each vertex of the simplex.
3) Compare the cost function for each vertex, and determine the lowest error "best" and highest error "worst" vertices.
4) Sequentially locating first the reflected, then, if necessary, the expanded, and then, if necessary, the contracted vertices; calculating for each of the corresponding cost function; and comparing it to the worst vertex. If, at any step, the cost function of the new trial point is less than the value at the worst vertex, then this vertex is substituted as a vertex in place of the current worst vertex.
5) If the process in step 4 does not yield a lower error value than the previous worst, then the other vertices are shrunken toward the best vertex.
6) At each stage of shrinking, the distances between vertices are calculated and compared to a set tolerance value to check if the simplex has become sufficiently small for the termination of the estimation. When the test criterion is reached, the previous best vertex becomes the solution.
7) At each stage of shrinking, the cost function values at the vertices are compared to a set minimum value to check if the error residual has become sufficiently small for the termination of the estimation. When the test criterion is reached, the previous best vertex becomes the solution.

III. PPD-IFM Algorithm Outline

The PPD-IFM algorithm makes use of the AMS source model, the simplified KF governing equations outlined in Table I, and the previously outlined IFM technique. In the implementation of the PPD-IFM algorithm, there are three parameters to be specified *a priori*: 1) The maximum possible length of the source wave $(T_{\max})$; 2) the maximum number of possible overlapping source waves $(N_{\max})$; and 3) the minimum time separation between the reflection coefficients $(RT_{\min})$. The parameter $T_{\max}$ is an approximate variable, and it typically does not exceed $2.5T$, where T is the corresponding period of the dominant frequency of the source wave. For example, the Ricker wave [5] has a time duration of approximately $1.5T$, the finite-difference source wave of Amini and Howie [11], [12] has an approximate source wave time length of $1.5T$, and the downhole seismic source waves in Figs. 3 and 5 have time durations of approximately $1.7T$ and $1.5T$, respectively. $T_{\max}$ is specified due to the fact that we are attempting to estimate the source wave, and it is only required to process $T_{\max}$ amount of seismogram data from the initial onset of the source wave.

Parameter $N_{\max}$ is required because it determines the maximum number of parameters that are to be estimated within the IFM portion of the PPD-IFM algorithm. Parameter $N_{\max}$ defines the maximum number of reflection coefficients within the source wave time span. $N_{\max}$ does not reflect the total number of reflection coefficients within the seismogram but the maximum number of reflection coefficients which can reside within the time duration of the source wave. This concept is shown in Fig. 8, where a source wave is superimposed upon a series of reflection coefficients. As shown in Fig. 8, there are a total of 15 reflection coefficients within the 110-ms time span. The source wave shown in Fig. 8 has a time duration of approximately 32 ms, and only five reflection coefficients can reside within that time span. Since it is very unlikely that there are more reflection coefficients in a source wave, the default value of $N_{\max}$ is set at five.

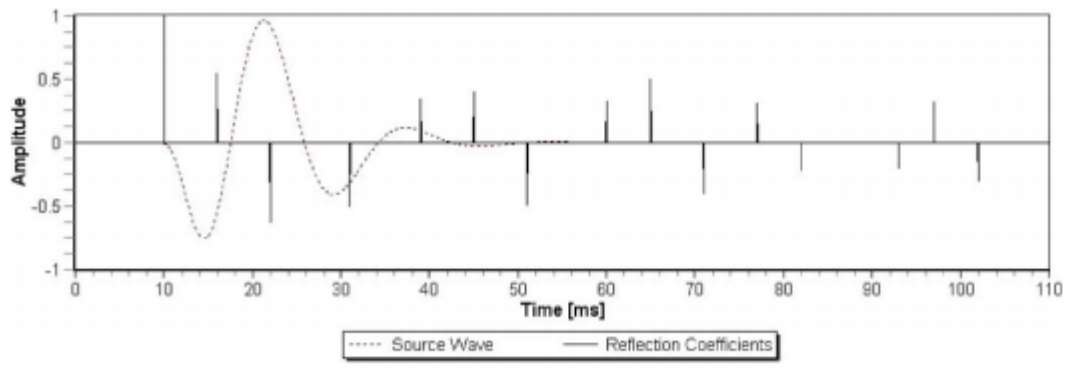

Fig. 8. Illustrating the concept behind parameters $T_{\max}$ and $N_{\max}$.

Parameter $RT_{\min}$ allows constraining of the PPD-IFM algorithm solution space. For example, the reflection coefficients $R_0, R_1, R_2, R_3, \ldots, R_N$ must arrive subsequently later within the time series (i.e., $t_1 < t_2 < t_3 \ldots, t_N$) based on the physics of reflection seismology. Parameter $RT_{\min}$ allows the investigator to set the minimum allowable time separation between the reflection coefficients. As expected, for smaller values of parameters $T_{\max}$ and $N_{\max}$ and for a larger value of $RT_{\min}$, there is a corresponding reduced CPU requirement for processing the seismic data.

In shallow and deep reflection seismology, it is reasonable to assume that there will be a maximum of three to four overlapping source waves recorded within the seismogram ($N_{\max} = 3$ or 4). For example, Sheriff and Geldart [19] demonstrate that the expected vertical resolution of a noise-free reflection seismic survey is $\lambda/4$, where λ defines the wavelength of the source wave. For shallow investigations (20–100 m), it is reasonable to assume a dominant compression source wave frequency (f) of approximately 100 Hz $(T = 1/f = 10$ ms) and a corresponding velocity (Vp) of 1500 m/s. Based on these parameters, the calculated vertical resolution is 3.75 m (note: $\lambda = V/f$). The associated two-way travel time (Δt) of the source wave for a vertical resolution of 3.75 m is 5 ms (i.e., $\Delta t = 2 * 3.75/V$). The assumed source wave time length of two times the period $(2 * T = 2/f)$ is 20 ms. This implies that there could be a maximum of three overlapping source waves for a vertical resolution of 3.75 m. A similar calculation can be made for a deep reflection (500 m to 5 Km) survey, where $V_p \approx 3000$ to 5000 m/s and $f \approx 50$ Hz[19].

The specification of parameter $RT_{\min}$ allows the investigator to exceed Sheriff's and Geldart's $\lambda/4$ vertical resolution and makes the PPD-IFM algorithm ideal in identifying thin bed layering. For example, if $V_P = 1500$ m/s and $f = 100$ Hz, then $\lambda = 15$ m. If $RT_{\min} = 3$ ms, the source wave travels 4.5 m. If we consider a two-way travel time, then the layer interval thickness would be 4.5 m$/2 = 2.25$ m. This exceeds Sheriff's and Geldart's defined resolution of a noise-free reflection seismic survey $(\lambda/4 = 3.75$ m) by 1.5 m or 40%. Alternatively, if

a minimum reflection coefficient separation of 2 ms is specified and a two-way travel is considered, then a layer thickness of 1.5 m could be resolved. This equates to a 60% improvement in the expected vertical resolution of 3.75 m.

If $Vp = 4000$ m/s and $f = 50$ Hz, $\lambda = 80$ m. In 3 ms, the source wave travels 12 m. If we consider a two-way travel time, then the layer interval thickness would be $12\ \text{m}/2 = 6$ m. This exceeds Sheriff's and Geldart's defined resolution of a noise-free reflection seismic survey ($\lambda/4 = 20$ m) by 14 m or 70%. Alternatively, if a minimum reflection coefficient separation of 2 ms is specified and a two-way travel is considered, then a layer thickness of 4 m could be resolved. This equates to an 80% improvement in the expected vertical resolution of 20 m.

The maximum resolution (i.e., minimum $RT_{\min}$ specification) capability of the PPD-IFM algorithm is dependent on the PPD-IFM input parameter values such as the user-specified dominant frequency analysis window and the properties of the additive measurement noise. Although $RT_{\min} \leq 3$ ms values have been typically specified when processing varying synthetic seismograms, it is the intention of the author to explore and quantify this issue further in a subsequent paper.

Fig. 2 shows the three fundamental source wave parameters of ω, t_{Offset}, and h. The reflection coefficients' parameters are the arrival times and corresponding amplitudes. If we assume a maximum of five overlapping source waves to be estimated, then the required 12 PPD-IFM parameters to be estimated are ω, t_{Offset} (note: the sinusoidal arrival time is defined as $t_0^{/} = t_0 + t_{\text{offset}}$), h, R_0, R_1, R_2, R_3, R_4, t_1, t_2, t_3, and t_4. These parameters are iteratively adjusted within the IFM DSM algorithm until the cost function is minimized. The desired parameter estimates are defined as those which minimize the cost function. The cost function is defined to be the rms difference between the estimated seismogram and the true seismogram over time window t_0 (source wave arrival time) to $t_0 + T_{\max}$.

In the KF portion of the PPD-IFM algorithm, the single state that is to be estimated is the AMT component of the AMS source wave. The overlapping source waves are modeled as known inputs based upon the IFM arrivals and amplitudes of the reflection coefficients and the proceeding time estimates of the AMT. In simplistic terms, the processed seismogram is assumed to be composed of up to five overlapping time invariant source waves, and we are attempting to estimate the AMT component of the source wave utilizing the simplified KF.

In discrete form, the AMS equation of (7) is given as

$$\text{AMS}_k = \text{AMT}_k \sin[2\pi f \Delta k + \varphi]. \tag{16}$$

In (16), k denotes the time index, f is the dominant frequency, Δ is the sampling rate, and φ is the phase of the AMS source wave. In [6], it is clearly outlined how the phase of the source wave is readily determined from the arrival time $t_0^{/} = t_0 + t_{\text{offset}}$ and the dominant frequency. The reflection coefficients are defined to be a scaled version of the maximum amplitude of the estimated source wave and are defined to reside within the bounds $0 \leq R \leq 1$. The overlapping source waves are processed in chronological order and are assumed to be offset by not less than the parameter $RT_{\min}$. The KF portion of the PPD-IFM algorithm is outlined in Table II.

As outlined in Table II, the KF PPD-IFM filter is utilized to determine the cost function for a particular set of source wave and reflection series input parameters. In addition to the requirement that the maximum resides within $1.5T$ of the onset of the source wave, there are several other AMT checks that can be made for code optimization (i.e., early exit from the KF algorithm) due to the fact the KF is a recursive filter. Some examples of the *in-line* checks which can be carried out are outlined as follows.

1) There should not be a widely fluctuating AMT.
2) A new maximum should not occur after *AMTmax*.
3) At time $T_{\max}$ from the arrival time (t_0) of the source wave, we would expect that the AMT amplitude should have decayed significantly from $\text{AMT}_{\max}$ (i.e., $< 5\%$).
4) There are minimum and maximum bounds on the decay of the source wave.

The sign of the reflection coefficients in Table II is determined *in-line* by processing the data over time span $RT_{\min}$ and by determining which sign $(\pm R)$ results in the minimum residual error over $RT_{\min}$.

There are three stages of analysis within the PPD-IFM algorithm. In the first two stages of analysis, a coarse sampling rate (Δc) is utilized, where there is minimum of 22 samples/T, with $T = 1/f$. The initial coarse sampling rate is implemented to considerably reduce the CPU requirements. The last stage of the analysis utilized the true sampling rate of the inputted time series.

The three stages of the PPD-IFM analysis are outlined as follows.

1) Utilize a coarse sampling rate (Δc) with the IFM portion of the PPD-IFM not implemented. Determine top $(S_1 = 400)$ source wave and reflection series parameter estimates which result in minimum cost function residuals. Sort error residuals from smallest to largest.
2) Based on the results in step1 $(S_1 = 400)$ and on a coarse sampling rate, determine top $(S_2 = 50)$ source wave and reflection series parameter estimates which result in minimum cost function residuals. In this stage of the analysis, the IFM algorithm is implemented. Sort error residuals from smallest to largest.
3) Based on the results in step 2 and on the true sampling rate, determine top $(S_3 = 10)$ source wave and reflection series parameter estimates which result in minimum cost function residuals. In this stage of the analysis, the IFM algorithm is again implemented. Sort error residuals from smallest to largest.

In steps 1 to 3 outlined earlier, $S_{1,2,3}$ denotes the total amount of model space samples for each stage of the analysis.

The PPD-IFM algorithm is implemented in three stages. This is due to the fact that there are many local minima of the cost function which can occur for various values of ω, t_{Offset}, h, R_0, R_1, R_2, R_3, R_4, t_1, t_2, t_3, and t_4. The first stage of the analysis optimally polls through the possible parameter values utilizing nested while loops, the iterative analysis windows (e.g., ± 2 Hz for f, ± 2 ms for arrival times, $0 \leq t_{\text{offset}} < T/2$, and $0 \leq R \leq 1$), and the user-specified minimum $(f_{\min})$

TABLE II
KF PPD-IFM FILTER FORMULATION

	Description	Mathematical Representation
1	Input parameters from IFM: ω, t_{Offset} (note: the sinusoidal arrival time is defined as $t_0' = t_0 + t_{offset}$), h, R_0, R_1, R_2, R_3, R_4, t_1, t_2, t_3 and t_4. $t_1' = t_1 + t_{offset}$, $t_2' = t_2 + t_{offset}$, $t_3' = t_3 + t_{offset}$, $t_4' = t_4 + t_{offset}$	The five possible overlapping source waves are denoted as $SW0_k$, $SW1_k$, $SW2_k$, $SW3_k$, & $SW4_k$. Set parameter AMT_EXP = FALSE Process time series from time $(note: t = \Delta k)$ $t = t_0$ to $t = t_0 + T_{\max}$
2	Initialize source for time index k. Calculate overlapping source waves at time index k based upon time value t. Note: linear interpolation is utilized when calculating $AMT_{t-\Delta t'}$ between available sample points.	$SW0_k = SW1_k = SW2_k = SW3_k = SW4_k = 0$ N = source wave index ($N = 0, 1, 2, 3, 4$). $\Delta t' = t_N - t_0$ If $t_N \le t < t_N'$ then $SWN_t = AMT_{t-\Delta t'} \times RN$ If $t_N' \le t$ then $SWN_t = AMT_{t-\Delta t'} \times RN \times \sin[2\pi ft + \varphi_N]$
3	Calculate measurement extrapolation and innovation (eqs. (13)&(14) in Table I).	$\hat{z}_k = SW0_k + SW1_k + SW2_k + SW3_k + SW4_k$ $\Delta_k = z_k - \hat{z}_k$
4	Obtain new estimate of the source AMT. Note: In the PPD-IFM algorithm there is no assumed extrapolation equation for the AMT.	$AMT_k = AMT_{k-1\|k-1} + \Delta_k / H_k$ If $t < t_0'$ then $H_k = R0$ If $t \ge t_0'$ then $H_k = R0 \times \sin[2\pi ft + \varphi_0]$ or $1/H_k = \textbf{\textit{cosecant}}[2\pi ft + \varphi_0]/R0$ note: $AMT_{k\|k-1} = AMT_{k-1\|k-1}$
5	In the PPD-IFM the maximum of the AMT or source wave is assumed to occur within time 1.5T ($T=1/f$).	Track AMT maximum (AMT_{MAX}). If the AMT maximum exceeds 1.5T then there is an early exit from the KF with an error flag.
6	When the AMT value drops below AMT_{MAX} at time index t_{exp}, then apply exponential decay estimate. AMT_EXP = TRUE	$AMT_k = AMT_{k-1} \times \exp^{-h(t-t\exp)}$
7	Based upon new estimate of AMT_k update $SW0_k$.	
8	Let k = k+1 & iterate to step 2. Skip steps 4 and 5 if AMT_EXP = TRUE.	
9	Calculate RMS error residual and return value to IFM algorithm.	$E = \sum_{k=k_0}^{k_0+k_1} \left[z_k - \begin{pmatrix} SW0_k + SW1_k + SW2_k \\ + SW3_k + SW4_k \end{pmatrix} \right]^2$ $E_{RMS} = \sqrt{E/k_1}$ note: $k_0 = t_0/\Delta$ & $k_1 = T_{\max}/\Delta$

and maximum ($f_{\max}$) dominant frequency values. For each iteration of the while loops, several samples are drawn from the source wave parameters of ω, t_{Offset}, and h and reflection arrival times and coefficients utilizing a Monte Carlo technique. Based on these samples, an error residual is calculated as outlined in Table II and is stored as previously described in step 2.

In stage 2 of the PPD-IFM, the top N_1 results of stage 1 are processed, utilizing the IFM algorithm. In this case, the analysis windows (e.g., $t_{1EST} - 2$ ms $\le t_{1EST} < t_{1EST} + 2$ ms) are specified around each parameter, several samples are drawn (utilizing the previously outlined Monte Carlo technique), and corresponding error residuals are calculated. The estimates which give the lowest 13 error residuals are utilized within the IFM algorithm for the purpose of specifying the initial simplex. Stage 3 of the PPD-IFM is identical to that outlined in stage 2, but in this case, the true sampling rate is utilized, and the top N_2 results of stage 2 are processed.

To further reduce the possible solution space of the PPD-IFM, two closely spaced seismograms are processed, simultaneously utilizing multithreading and making use of the standard dual-core processor technology. For example, in a typical downhole seismic investigation, the receivers are offset by 1 m [12]–[16]. This 1-m offset is equivalent to a 10-ms source time offset for a medium velocity of 100 m/s. It is highly likely that two source waves that are offset by 10 ms are identical. When processing two seismic traces simultaneously, the PPD-IFM algorithm, after stages 2 and 3, determines the top source wave estimates where the weighted rms difference between the estimated seismograms and the true seismograms over time window t_0 (source wave arrival time) to $t_0 + T_{\max}$ are minimized. The weight of the cost function is defined as the

absolute sum difference between the source wave parameters (i.e., ω, t_{Offset}, h, and time location $T_{\text{AMT max}}$ of AMT_{max}). The weight on the cost function is given as

$$\text{weight} = \text{abs}(f_1 - f_2) + \text{abs}(T1_{\text{AMT max}} - T2_{\text{AMT max}}) + \text{abs}(h_1 - h_2) + \text{abs}(t_{\text{offset1}} - t_{\text{offset2}}). \quad (17)$$

The minimum and maximum source wave attenuation values are automatically estimated within the PPD-IFM algorithm based on the user-specified minimum $(f_{\min})$ and maximum $(f_{\max})$ dominant frequency windows of the source.

A. Minimum Attenuation Value

The exponential decay is defined as $X = X_0 e^{-h\Delta t}$. If the amplitude of the AMT is calculated when it decays to 0.05 (5%) of the maximum value AMT_{MAX}, we have $0.05 = e^{-h\Delta t}$ or $h\Delta t = 3$. Since it can be assumed that the maximum source length is $2.5T$ and that it will take at least $0.25T$ to reach AMT_{MAX} from t_0 (as is the case with every sine wave), the time for the source wave to decay to 5% of AMT_{MAX} is therefore at most $2.25T$. This means that

$$h_{\min} = 3/2.25T_{\max} = 1.333 f_{\min}$$

if $f_{\min} = 50$ Hz then $h_{\min} = 66.665/\text{sec}$ or $0.066665/\text{ms}$.

B. Maximum Attenuation Value

Based on analytical source wave representations and numerous real data examples it can be assumed that the time for the source wave to decay to 5% of AMT_{MAX} is at least $0.5T$. This means that

$$h_{\max} = 3/0.5T_{\min} = 6 f_{\max}$$

if $f_{\max} = 60$ Hz then $h_{\max} = 360/\text{s}$ or $0.36/\text{ms}$.

IV. PPD-IFM Simulation Results

The implementation and performance of the PPD-IFM algorithm is demonstrated by considering the analysis of two challenging synthetic seismograms. The seismograms are challenging due to the fact that there are five closely spaced reflection coefficients with dipoles in a high measurement noise environment. The PPD-WE [6] algorithm would have difficulty in processing this data set. This is due to the fact that the seismograms have phase components that are similar to that of the source wave to be extracted and the gradual decrease in the quality of the estimated source waves due to the propagation of errors [6]. The first seismogram was generated by convolving the Berlage wave shown in Fig. 1 with the reflection coefficients outlined in Fig. 9 to give the output shown in Fig. 10. The second seismogram is generated by convolving the Berlage wave in Fig. 1 with the reflection series shown in Fig. 11. The resulting seismogram is shown in Fig. 12. Table III outlines the reflection series parameters of the arrival time and amplitude for seismograms 1 and 2.

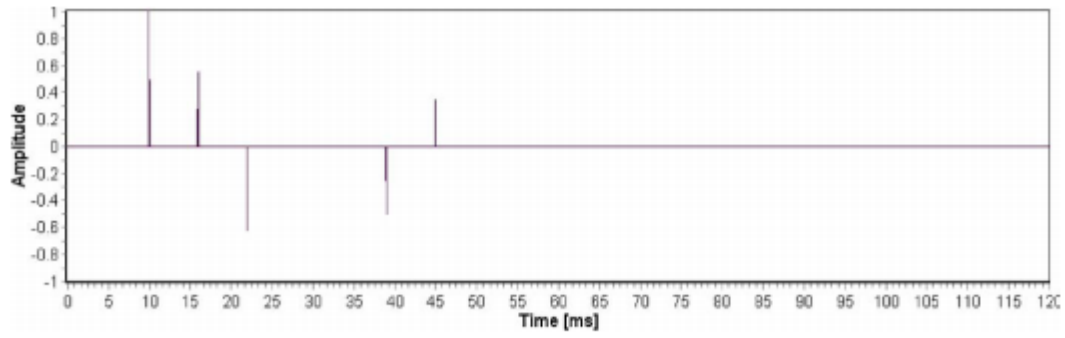

Fig. 9. Seismogram 1 reflection coefficients.

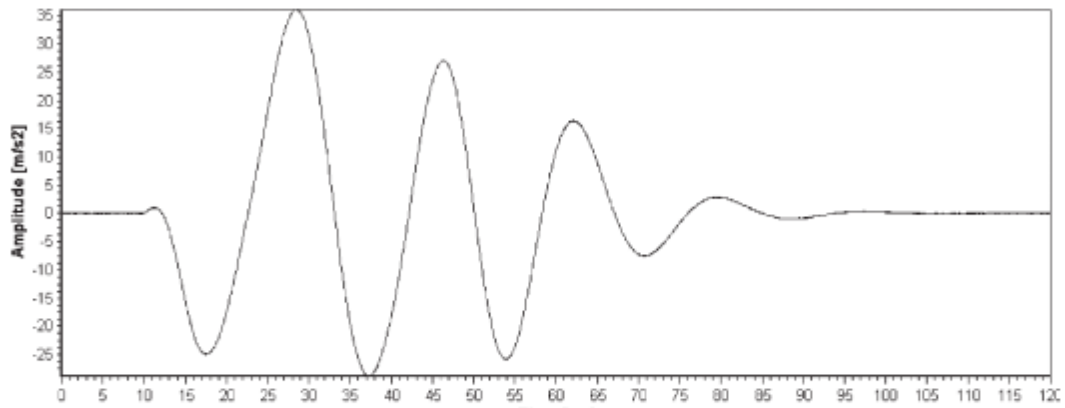

Fig. 10. Output after convolving the Berlage wave in Fig. 1 with the reflection coefficients shown in Fig. 9.

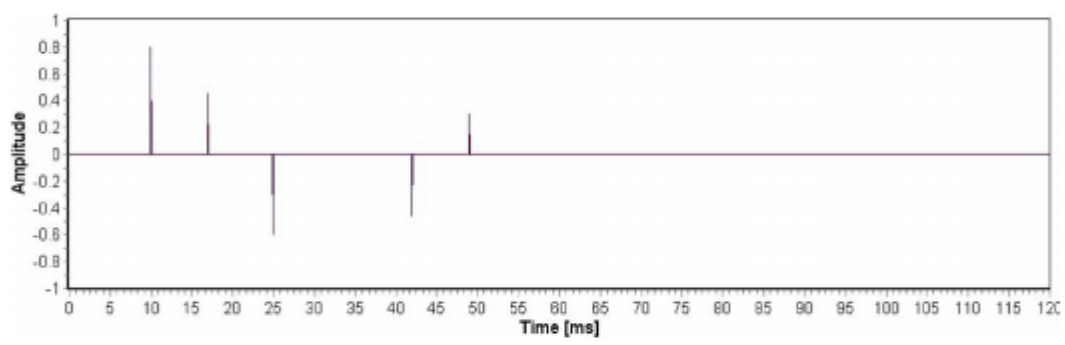

Fig. 11. Seismogram 2 reflection coefficients.

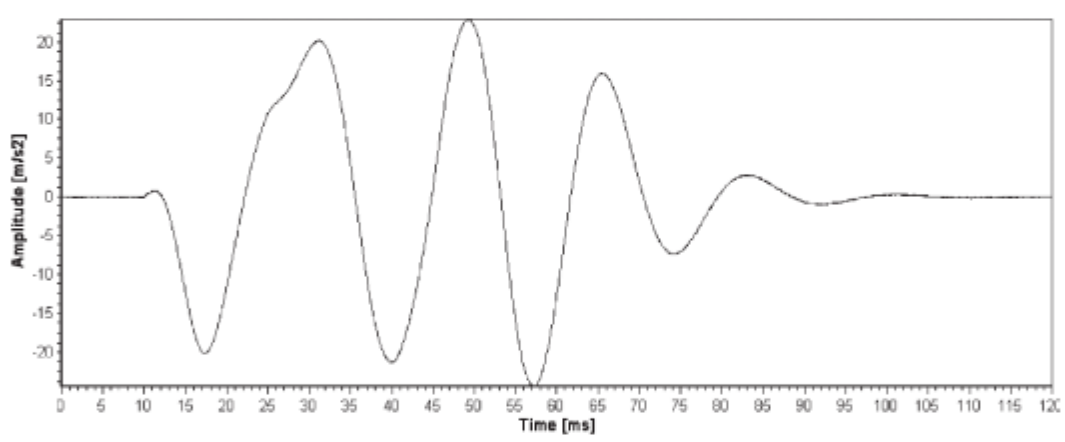

Fig. 12. Output after convolving the Berlage wave in Fig. 1 with the reflection coefficients shown in Fig. 11.

TABLE III
Reflection Series Parameters

Seismogram 1		Seismogram 2	
Reflection Coefficients		Reflection Coefficients	
Time [ms]	Amplitude	Time [ms]	Amplitude
10	1.0	10	0.8
16	0.55	17	0.45
22	-0.625	25	-0.6
39	-0.5	42	-0.46
45	0.35	49	0.3

As shown in Figs. 9 and 11 and Table III, the reflection series for seismograms 1 and 2 is very similar, with minor variations. The similarity of the reflection series is to reflect the case where we have recorded the seismic traces from two relatively closely spaced receivers. This allows the implementation of the weighted cost function. Although there are minor variations between the reflection series of seismograms 1 and 2, the

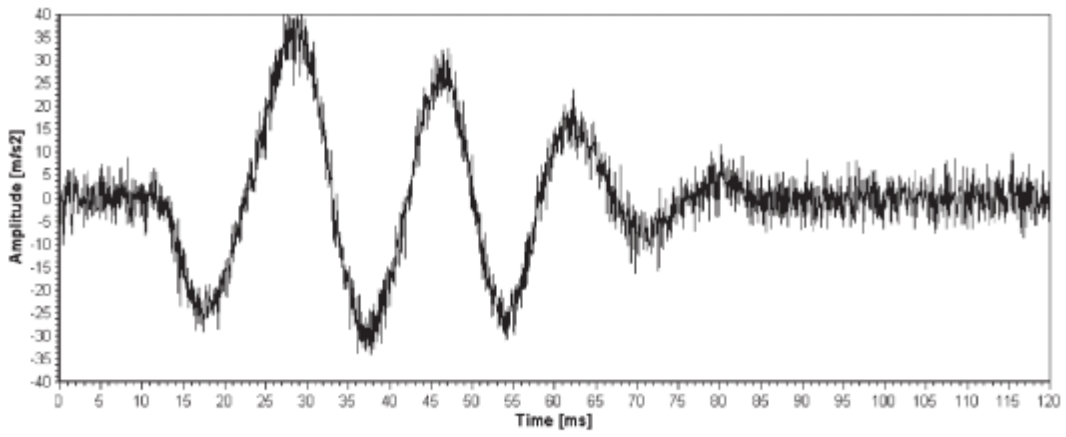

Fig. 13. Seismogram of Fig. 10 with the additive Gauss–Markov measurement noise.

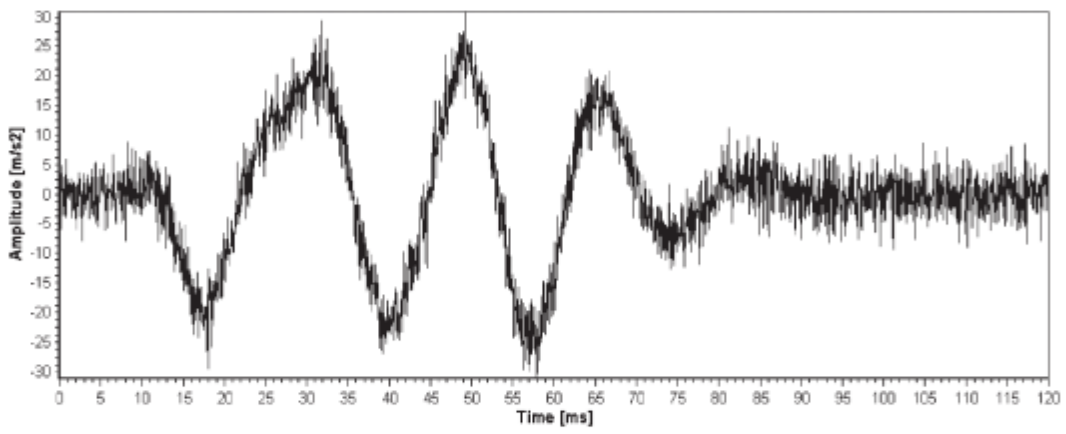

Fig. 14. Seismogram of Fig. 12 with the additive Gauss–Markov measurement noise.

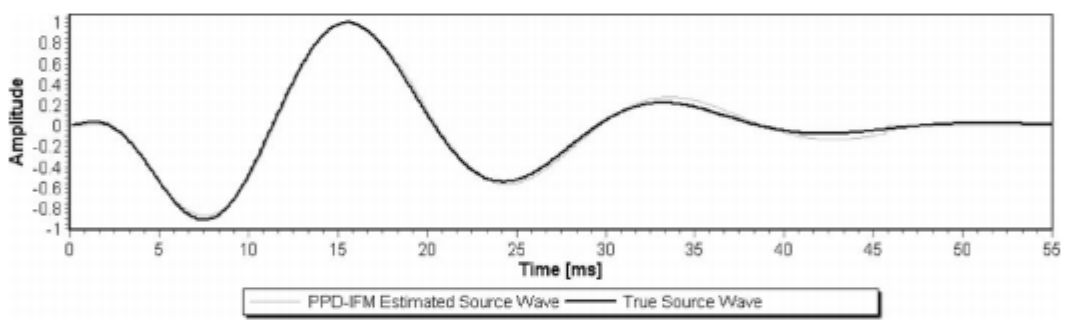

Fig. 15. PPD-IFM estimated source wave superimposed upon the true source wave for the time series shown in Fig. 13.

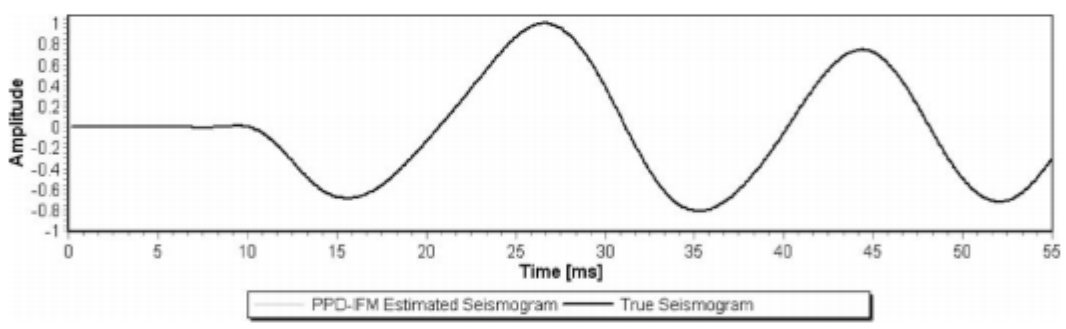

Fig. 16. PPD-IFM estimated normalized seismogram superimposed upon the true normalized seismogram for the time series shown in Fig. 13.

resulting seismograms have significant differences, as shown in Figs. 10 and 12. The synthetic seismograms shown in Figs. 10 and 12 have Gauss–Markov [6], [8], [9] measurement noise added, with the variance and time constants set to 10 units$^2/$s^2 and 0.01 ms, respectively. Figs. 13 and 14 show Figs. 10 and 12, respectively, with the additive Gauss–Markov noise.

The noisy seismic traces shown in Figs. 13 and 14 are preprocessed with an eighth-order Butterworth 200-Hz low-pass zero-phase digital filter applied. The filtered seismograms are then fed into the PPD-IFM algorithm, with the parameters $f_{\min}$, $f_{\max}$, and $RT_{\min}$ set to 40 Hz, 60 Hz, and 3 ms, respectively.

The estimated PPD-IFM normalized source wave for seismogram 1 is shown in Fig. 15, superimposed upon the true-noise-free (i.e., no additive Gauss-Markov measurement noise) normalized source wave. Fig. 16 shows the estimated normalized seismogram superimposed upon the true normalized seismogram with a corresponding rms error of 0.06 units. Fig. 17 shows the error residuals for the PPD-IFM estimated normalized source wave and true normalized source wave (as shown in Fig. 15), and the PPD-IFM estimated normalized seismogram and the true normalized seismogram (as shown in Fig. 16). The PPD-IFM estimated reflection coefficients (superimposed upon the true reflection coefficients) are shown in Fig. 18 and are quantitatively compared with the true values in Table IV. As shown in Figs. 15–18 and Table IV, the PPD-IFM algorithm was able to obtain accurate estimates of the source wave and reflection series for the seismogram shown in Fig. 13 and utilizing a weighted cost function.

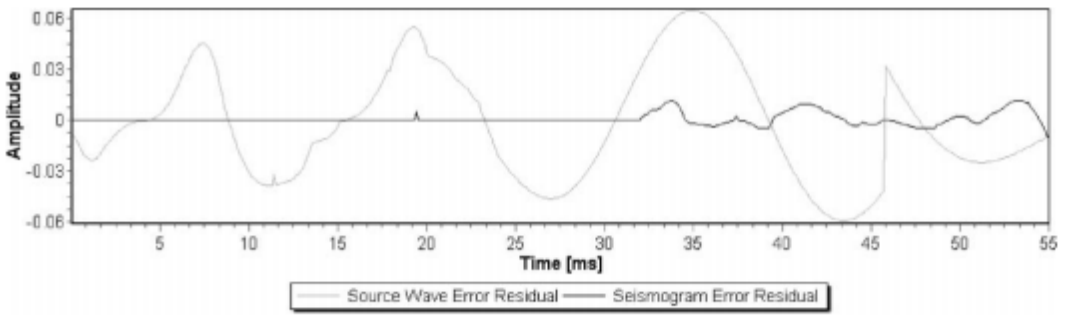

Fig. 17. Error residuals for the PPD-IFM estimated source wave and true source wave, and the PPD-IFM estimated seismogram and true seismogram for the time series shown in Fig. 13.

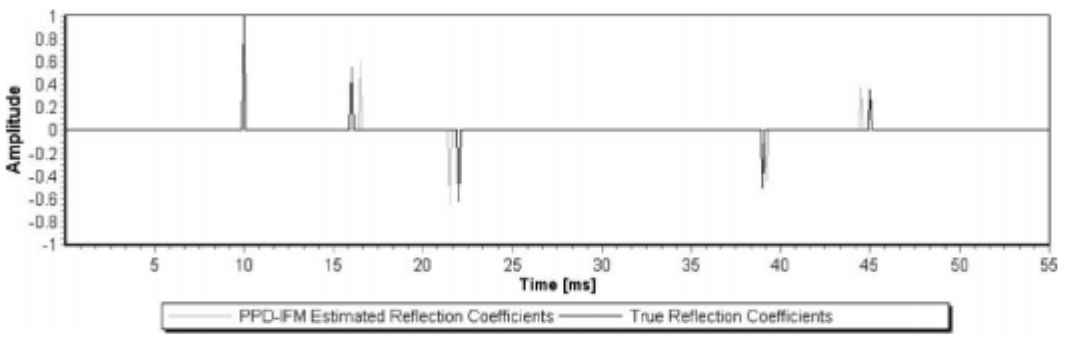

Fig. 18. PPD-IFM estimated reflection series superimposed on the true reflection series for the time series shown in Fig. 13.

The estimated PPD-IFM normalized source wave for seismogram 2 is shown in Fig. 19, superimposed upon the true normalized source wave. Fig. 20 shows the estimated normalized seismogram superimposed upon the true normalized seismogram with a corresponding rms error of 0.05 units. Fig. 21 shows the error residuals for the PPD-IFM estimated source wave and true source wave (as shown in Fig. 19), and the PPD-IFM estimated normalized seismogram and the true normalized seismogram (as shown in Fig. 20). The PPD-IFM estimated reflection coefficients for the seismogram shown in Fig. 14 are shown (superimposed upon the true reflection coefficients) in Fig. 22 and are quantitatively compared with the true values in Table V. The PPD-IFM algorithm again obtained very accurate source waves and reflection series estimates when processing the time series shown in Fig. 14 and when implementing a weighted cost function.

The source wave estimates shown in Figs. 15 and 19 could be utilized to deconvole the source wave from the seismogram utilizing the water level technique (WLT) [1], [6] so that the complete reflection series is obtained. The implementation of the WLT is a fast and simple approach if there is a minimal source wave variation within the seismogram. If a significant source wave variation occurs within the seismogram, then a recursive PPD-IFM approach could be utilized. In this

TABLE IV
COMPARING ESTIMATED AND TRUE REFLECTION SERIES PARAMETERS FOR SEISMOGRAM 1

True Reflection Coefficients		Estimated Reflection Coefficients		Absolute Errors	
Time [ms]	Amplitude	Time [ms]	Amplitude	Time [ms]	Amplitude
10	1.0	10	0.99	0	0.01
16	0.55	16.5	0.60	0.5	0.05
22	-0.625	21.5	-0.65	0.5	0.025
39	-0.5	39.2	-0.44	0.2	0.06
45	0.35	44.5	0.37	0.5	0.02

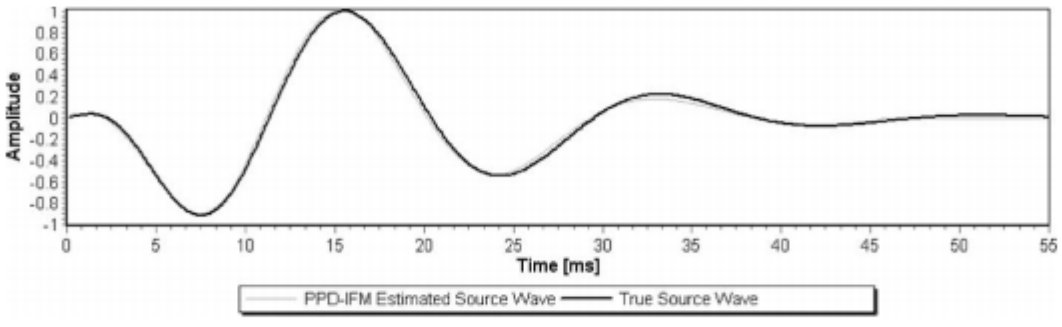

Fig. 19. PPD-IFM estimated source wave superimposed upon the true source wave for the time series shown in Fig. 14.

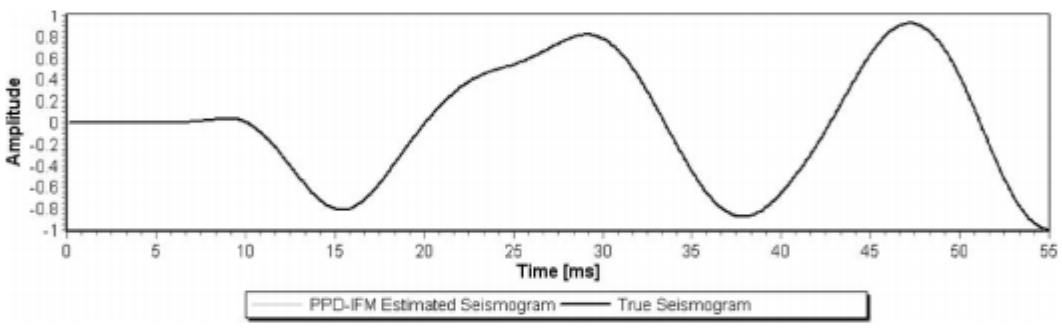

Fig. 20. PPD-IFM estimated normalized seismogram superimposed upon the true normalized seismogram for the time series shown in Fig. 14.

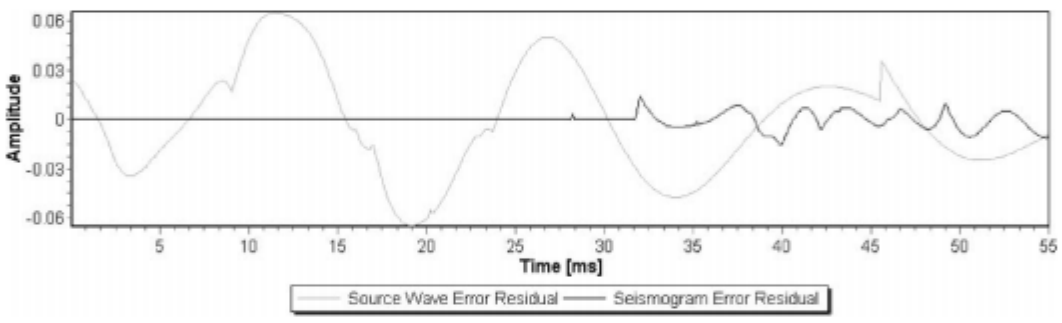

Fig. 21. Error residuals for the PPD-IFM estimated source wave and true source wave, and the PPD-IFM estimated seismogram and true seismogram for the time series shown in Fig. 14.

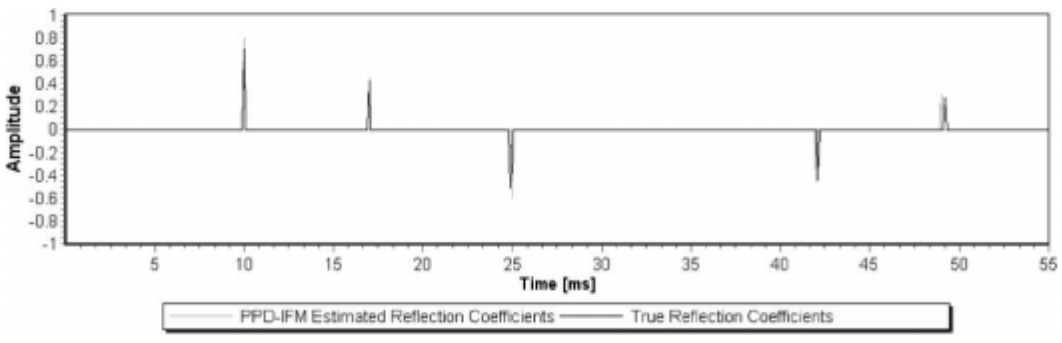

Fig. 22. PPD-IFM estimated reflection series for the time series shown in Fig. 16.

case, the PPD-IFM algorithm is applied recursively, where the PPD-IFM estimated seismograms over time $T_{\max}$ (as shown in Figs. 16 and 20) are sequentially and chronologically extracted from the seismogram under analysis until the total seismogram has been processed and the complete reflection series is estimated. Alternatively, the WLT technique could initially be implemented until a time index $t*$ is identified, where the reflection coefficients change shape (signifying a source wave time variance [1], [6]). The PPD-IFM algorithm could then be reapplied at time index $t*$.

V. CONCLUSION

Seismic deconvolution is the most widely utilized signal enhancement technique in seismic signal processing. Ideally, by deconvolving the source wave from the recorded time series data, only the reflection coefficients remain. A very challenging problem in seismic deconvolution is blind deconvolution. In this case, both the source wave and reflection coefficients are assumed unknown.

This paper has outlined a more powerful formulation of a previously published concept in BSD, referred to as PPD. This new filter formulation is referred to as the PPD-IFM algorithm. In the PPD-IFM filter formulation, an IFM algorithm is incorporated, which allows for a significantly more accurate approach in estimating the source wave and corresponding reflection series and addresses the limitations of the previous versions of the PPD algorithm, such as the requirement of specifying the phases of the overlapping source waves *a priori*.

Full details on the formulation and implementation of PPD-IFM algorithm are provided within this paper. An important component of the PPD-IFM algorithm is the modeling of the source wave as an AMS. The AMS is demonstrated to be a highly robust and accurate approximation of many analytical and real representations of seismic source waves. In general terms, in the PPD-IFM algorithm, the overlapping source waves are treated as known inputs within a simplified Kalman filter formulation based on the current source wave and reflection series IFM parameter estimates. The source wave and reflection series parameters are obtained by iteratively minimizing a cost function that is defined to be the rms weighted difference between the measured seismogram and the synthesized seismogram within the IFM algorithm. It is assumed that there are very low measurement noise and process noise due to the fact that the seismic data can be preprocessed so that the signal-to-noise ratio is increased significantly.

The IFM technique that is utilized within the PPD-IFM algorithm is the DSM. The DSM in multidimensions has the important property of not requiring derivatives of function evaluations, and it can minimize nonlinear functions of more than one independent variables. The specification of parameter $RT_{\min}$ (the minimum time separation between reflection coefficients) allows the investigator to exceed Sheriff's and Geldart's $\lambda/4$ vertical resolution and makes the PPD-IFM algorithm ideal in identifying thin bed layering. Due to the fact that the KF is a recursive filter, there are AMT checks that can be made for code optimization (i.e., early exit from the KF algorithm). Examples

TABLE V
COMPARING ESTIMATED AND TRUE REFLECTION SERIES PARAMETERS FOR SEISMOGRAM 2

True Reflection Coefficients		Estimated Reflection Coefficients		Absolute Errors	
Time [ms]	Amplitude	Time [ms]	Amplitude	Time [ms]	Amplitude
10	0.8	10	0.72	0	0.08
17	0.45	17	0.42	0.0	0.03
25	-0.6	25	-0.51	0.0	0.09
42	-0.46	42	-0.44	0.0	0.02
49	0.3	49	0.28	0.0	0.02

of the *in-line* checks that can be carried out were outlined in this paper.

The implementation and performance of the PPD-IFM algorithm was demonstrated by considering very challenging synthetic seismograms which contained high variance Gauss–Markov measurement noise. The seismograms were challenging due to the fact that there were five closely spaced reflection coefficients with dipoles in a high measurement noise environment. It was shown that the PPD-IFM algorithm was able to obtain accurate estimates of the source wave and reflection series for the noisy seismograms.

REFERENCES

[1] T. J. Ulrych and M. D. Sacchi, *Information-Based Inversion and Processing With Applications*, 1st ed. Amsterdam, The Netherlands: Elsevier, 2005.

[2] R. E. Sheriff and L. P. Geldart, *Exploration Seismology*, vol. 2, 2nd ed. Cambridge, U.K.: Cambridge Univ. Press, 1983, p. 44.

[3] J. M. Mendel, *Optimal Seismic Deconvolution an Estimation-Based Approach*. San Diego, CA: Academic, 1983.

[4] J. M. Mendel, *Lessons in Estimation Theory for Signal Processing, Communications, and Control*. Englewood Cliffs, NJ: Prentice-Hall, 1995.

[5] E. Baziw and T. J. Ulrych, "Principle phase decomposition—A new concept in blind seismic deconvolution," *IEEE Trans. Geosci. Remote Sens.*, vol. 44, no. 8, pp. 2271–2281, Aug. 2006.

[6] E. Baziw, "Implementation of the principle phase decomposition algorithm," *IEEE Trans. Geosci. Remote Sens.*, vol. 45, no. 6, pp. 1775–1785, Jun. 2007.

[7] Z. Peng, Y. Li, W. Wei, Z. He, and D.-J. Li, "Nonlinear AVO inversion using particle filter," *Chin. J. Geophys.*, vol. 51, no. 4, pp. 862–871, 2008.

[8] E. Baziw, "Real-time seismic signal enhancement utilizing a hybrid Rao–Blackwellized particle filter and hidden Markov model filter," *IEEE Geosci. Remote Sens. Lett.*, vol. 2, no. 4, pp. 418–422, Oct. 2005.

[9] E. Baziw and I. Weir-Jones, "Application of Kalman filtering techniques for microseismic event detection," *Pure Appl. Geophys.*, vol. 159, no. 1–3, pp. 449–471, Jan. 2002.

[10] E. Baziw, B. Nedilko, and I. Weir-Jones, "Microseismic event detection Kalman filter: Derivation of the noise covariance matrix and automated first break determination for accurate source location estimation," *Pure Appl. Geophys.*, vol. 161, no. 2, pp. 303–329, Feb. 2004.

[11] A. Amini and J. A. Howie, "Numerical simulation of downhole seismic cone signals," *Can. Geotechnical J.*, vol. 42, no. 2, pp. 574–586, 2005.

[12] E. Baziw, "State-space seismic cone minimum variance deconvolution," in *Proc. 2nd Int. Conf. Geotechnical Site Characterization (ISC-2)*, 2004, vol. 1, pp. 835–843.

[13] R. G. Campanella, F. T. C. Robertson, and D. Gillespie, "Seismic cone penetration test," in *Proc. INSITU. ASCE Geotechnical Special Publication, no. 6*, 1986, pp. 116–130.

[14] E. Baziw, J. Tichy, and G. de Caprona, "Data acquisition in seismic cone penetration testing," in *Proc. 3rd Int. Symp. ITASCE*, Argonne, IL, Sep. 2000, pp. 69–72.

[15] E. Baziw, "Digital filtering techniques for interpreting seismic cone data," *J. Geotechnical Eng.*, vol. 119, no. 6, pp. 998–1018, Jun. 1993.

[16] E. Baziw, "Derivation of seismic cone interval velocities utilizing forward modeling and the downhill simplex method," *Can. Geotechnical J.*, vol. 39, no. 5, pp. 1181–1192, Oct. 2002.

[17] J. A. Nelder and R. Mead, "A simplex method for function optimization," *Comput. J.*, no. 7, pp. 308–313, 1965.

[18] J. B. Vance, F. P. Hassani, and M. Praviz, "Improved determination of microseismic source location using a simplex technique," *IEEE Trans. Ind. Appl.*, vol. 24, no. 4, pp. 666–671, Jul./Aug. 1988.

[19] R. E. Sheriff and L. P. Geldart, *Exploration Seismology*, vol. 1, 1st ed. Cambridge, U.K.: Cambridge Univ. Press, 1982, pp. 117–119.

Erick Baziw (M'05–SM'08) received the B.A.Sc. degree in geophysics engineering, the M.A.Sc. degree in geotechnical engineering, and the Ph.D. degree in geophysics time series analysis from the University of British Columbia, Vancouver, BC, Canada, in 1986, 1988, and 2007, respectively.

His research interests include Bayesian recursive estimation, signal processing, and imaging, with a particular emphasis on blind seismic deconvolution, passive seismology, site characterization, seismic tomography, and instrument modeling.

Dr. Baziw is a Registered Professional Engineer in geophysics and software engineering.